A Bose-condensed, simultaneous dual-species Mach–Zehnder atom interferometer

2014 New J. Phys. 16 073035

(http://iopscience.iop.org/1367-2630/16/7/073035)

New Journal of Physics
The open access journal at the forefront of physics
Deutsche Physikalische Gesellschaft DPG | IOP Institute of Physics

A Bose-condensed, simultaneous dual-species Mach–Zehnder atom interferometer

C C N Kuhn, G D McDonald, K S Hardman, S Bennetts, P J Everitt, P A Altin, J E Debs, J D Close and N P Robins

Quantum Sensors and Atomlaser Lab, Department of Quantum Science, Australian National University, Canberra 0200, Australia
E-mail: nick.robins@anu.edu.au

Received 24 January 2014, revised 28 April 2014
Accepted for publication 28 May 2014
Published 24 July 2014

New Journal of Physics **16** (2014) 073035

doi:10.1088/1367-2630/16/7/073035

Abstract

This paper presents the first realization of a simultaneous ^{87}Rb–^{85}Rb Mach–Zehnder atom interferometer with Bose-condensed atoms. A number of ambitious proposals for precise terrestrial and space based tests of the weak equivalence principle rely on such a system. This implementation utilizes hybrid magnetic-optical trapping to produce spatially overlapped condensates with a repetition rate of 20 s. A horizontal optical waveguide with co-linear Bragg beamsplitters and mirrors is used to simultaneously address both isotopes in the interferometer. We observe a non–linear phase shift on a non-interacting ^{85}Rb interferometer as a function of interferometer time, T, which we show arises from inter-isotope scattering with the co-incident ^{85}Rb interferometer. A discussion of implications for future experiments is given.

Keywords: atom interferometry, Bose–Einstein condensation, Bragg diffraction, atom optics

1. Introduction

Many decades of research have yet to unify the theory of gravity with the other fundamental interactions. It is conceivable that gravity is simply a classical field [1], however most theorists have pursued a quantization of gravity as the unifying theory [2]. Typically, these unifying

theories imply a violation of general relativity [3]. A number of ambitious experiments have been proposed to provide experimental data to test, and exclude or confirm, new theories.

Atom interferometers provide an ideal platform for these experiments [4–7], providing ultra-high resolution absolute measurements of gravity [8]. For example, simultaneously comparing a measurement of the acceleration due to gravity of two different atomic species allows a direct test of the weak equivalence principle (WEP) of general relativity. Indeed, large investments and spectacular progress have already been made in Europe and the US, most notably by the ESA projects Q-WEP and STE-QUEST in Europe [9–12], and the Stanford drop tower project [4]. The European teams, in particular, have made outstanding contributions to microgravity tests and the robustness of atom interferometry infrastructure [13, 14]. A feature of the proposed experiments, both terrestrial and space based, is the use of a dual isotope ^{87}Rb-^{85}Rb Bose–Einstein condensate (BEC) atom interferometer. A BEC based source allows direct manipulation of momentum width and spatial profile through modification of trapping potentials and scattering length [15]. The phase transition from a thermal cloud to a BEC produces a sudden and dramatic change in momentum width (with an equivalent classical gas temperature in the 10's of pK), a uniform and symmetric spatial profile (advantageous for reducing technical effects such as Coriolis shifts [16]), and an increased spatial coherence [17] (advantageous for maintaining fringe visibility in the presence of technical noise). These are all critical factors contributing to achieving a signal in long interrogation time interferometry. Additionally, the use of two isotopes suppresses common mode and platform noise by a predicted factor of 4×10^8 [12]. A very recent experiment demonstrated a simultaneous ^{87}Rb–^{85}Rb atom interferometer based on a laser cooled thermal source and Raman transitions, showed a factor of 550 common-mode noise rejection [18].

This paper demonstrates the first simultaneous Mach–Zehnder atom interferometer based on Bose-condensed sources of ^{87}Rb and ^{85}Rb. A simplified trapping apparatus, consisting of only two magnetic coils and a crossed dipole trap, is used to produce simultaneous BEC of ^{87}Rb and ^{85}Rb. A schematic of the trap and beam orientations is shown in figures 1(a) and (b). In order to study interferometry in quasi-expanded clouds (an approximation to the freely expanded clouds in space and long-drop terrestrial systems), the BECs are then loaded into a horizontal optical waveguide. An atom interferometer is constructed from co-linear counter propagating laser beams configured to drive Bragg transitions between momentum states. It is shown that s-wave inter-isotope scattering leads to a relative phase shift between the two isotopes. In addition to dual isotope interferometry for WEP tests, ^{85}Rb offers a number of intriguing possibilities for atom interferometry. The tuneable s-wave scattering of the ^{85}Rb condensate allows control of the mean-field phase shift associated with condensate atom interferometers [19], allowing interactions to be switched off. This has been demonstrated in the context of lattice based Bloch oscillations [20, 21]. This work provides the first such demonstration in a Mach–Zehnder atom interferometer. Both the dual-species and non-interacting condensate interferometers provide important data for both future space missions and terrestrial high precision measurements.

This paper is organized as follows. The apparatus is first described, focusing on the components and techniques that simplify production of ^{85}Rb condensates. The tuneable nature of the ^{85}Rb scattering length is demonstrated in both the crossed dipole trap and the waveguide. Results are then presented for a simultaneous Bose-condensed ^{87}Rb–^{85}Rb Mach–Zehnder atom interferometer and a non-interacting ^{85}Rb atom interferometer. The paper concludes with a discussion pertinent to the applications of this technique to proposed equivalence principle tests.

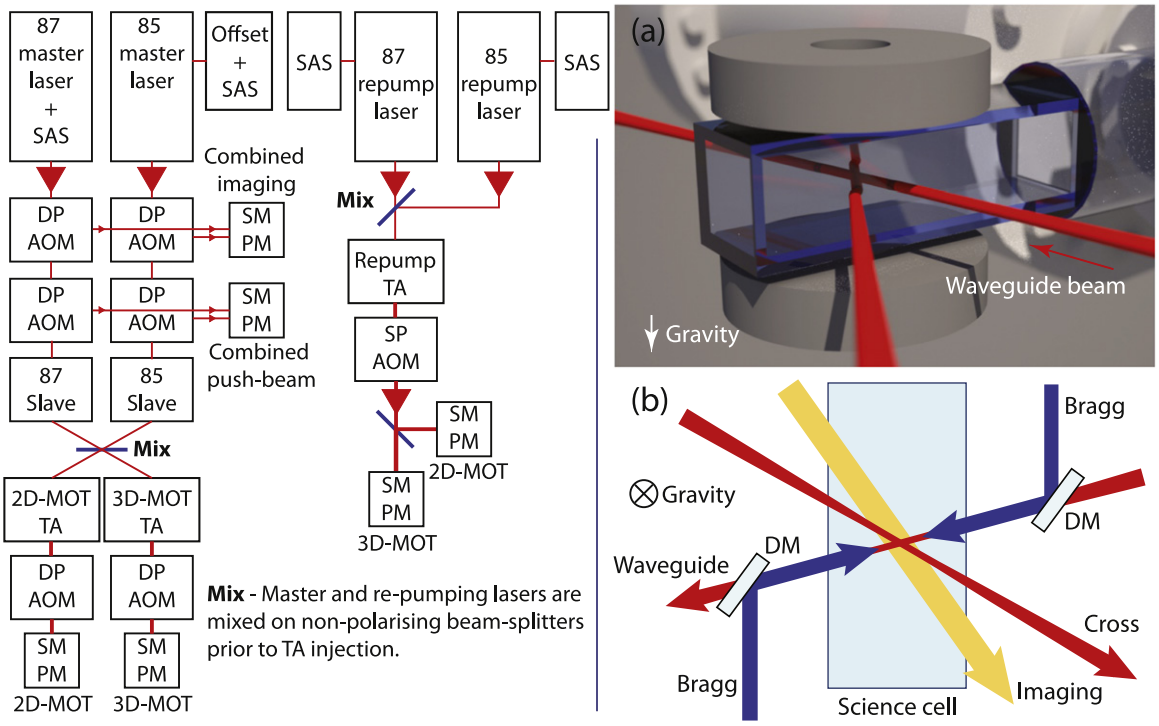

Figure 1. Left frame: schematic of the setup used to generate the laser light used in the experiment. Saturated absorption spectrometer (SAS), Single mode polarization maintaining fibre (SM PM), tapered amplifier (TA). The double pass acousto-optic modulator (DP-AOM) setup sites the AOM and retro-reflection mirror a focal length away from the centre lens. Right frame: (a) a simplified rendering of the experiment, showing the key hardware for producing the dual condensates. An ultra-high vacuum glass cuvette, quadrupole/Feshbach coils and the crossed dipole trapping beams. Not shown are the coincident two-colour MOT beams and the orthogonal absorption imaging systems. The glass cell is 3 cm × 3 cm × 10 cm on its outside edges. Right frame: (b) a schematic of the layout of the beam paths. DM—dichroic mirror. The second imaging beam path has been omitted to avoid clutter in the schematic.

2. Apparatus

The primary components of our experiment are a single set of low current (∼15A) coils that can be dynamically configured to produce either a Helmholtz or quadruple configuration magnetic field, and two separate 20 W laser beams that cross with large (∼100 μm) waists near the centre of the two coils. This design, based on ideas from the ^{87}Rb team at JQI [22, 23], is a far simpler setup than our previous ^{85}Rb apparatus [24]. Not surprisingly, this simplified system has many benefits, including much improved optical access and higher stability and repeatability in the condensate number.

The experiment is based around a compact vacuum system described previously [24]. The basic optical design of the experiment has been retained as well, utilizing a 2D-magneto-optical trap (2DMOT) to load the primary 3DMOT via a pair of co-propagating push beams. The setup used to produce the laser light is illustrated in a block diagram in figure 1. Four different frequencies of light are required for laser cooling of the two rubidium isotopes. The appropriate frequencies lie conveniently within a band of 6.8 GHz at 380 THz, easily accessible by readily

available external cavity diode lasers. Four separate lasers, one for each of the primary trapping and re-pumping transitions are used, each running at about 40 mW (post isolator). This configuration has proved to provide the best stability in the total and relative atom numbers in the dual condensates. We have found that sidebands added via diode modulation, external phase modulators or acousto-optic modulators (AOM) have so far proved less stable than this configuration, primarily due to alignment, temperature and polarization sensitivity [25]. By means of an AOM in the ^{85}Rb master locking loop, both trapping lasers are locked with the same offset from the $|F=2\rangle \rightarrow |F'=3\rangle$ and $|F=3\rangle \rightarrow |F'=4\rangle$ cooling transitions for ^{87}Rb and ^{85}Rb, respectively. The master lasers provide light for the push and imaging beams and for injection locking two separate free running diodes (running at 60 mW each). These injection locked lasers are mixed on a non-polarizing beamsplitter and used to seed two tapered amplifiers (TA). By varying the alignment, mode matching and relative input powers, the output from the TA's are optimized to contain an appropriate ratio of the cooling light for two isotopes in the 2/3D MOTs. Subsequent AOMs are used to rapidly vary the frequency and intensity of the light used for both MOTs, including shuttering. Finally, all light is guided to the experiment head in high quality, single-mode, polarization-maintaining optical fibers. Repump light is produced in much the same way. Both repump lasers are locked to saturated absorption cross-over resonances with the nearly the same offset (~78 MHz) from the re-pumping transitions $|F=1\rangle \rightarrow |F'=2\rangle$ and $|F=2\rangle \rightarrow |F'=3\rangle$ for ^{87}Rb and ^{85}Rb, respectively. The output from the repump lasers is mixed on a non-polarizing beamsplitter and one port is used to inject a TA. Post-TA, the light is split through two separate single-pass AOMs and sent to the 2/3D MOTs. Total trapping powers are 100 mW and 120 mW in the 3D and 2DMOTs, respectively, with approximately 15% of that power at the ^{85}Rb trapping frequency. Repump powers are ~25 mW for each species in each MOT. The main non-common fluctuation that can occur in dual frequency MOTs is through birefringent polarization instability in the single mode polarization maintaining fibre coupling light to the experiment. The laser setup is designed to minimise non-common fluctuations between the cooling lasers by combining them with co-linear polarization prior to TA injection. This is a critical factor in obtaining good stability in the final condensate atom numbers [25–27].

The magnetic field for the 3DMOT, quadrupole magnetic trap and for accessing the ^{85}Rb Feshbach resonance is generated by a single set of coils. The coils are driven by a custom-built, closed-loop stabilization circuit, providing a measured absolute RMS stability of better than 1:10^6 at a current of 15A (this corresponds to approximately 10 μG stability around the Feshbach resonance). At all times, the current runs in series through the two coils. High speed switching is provided by an integrated capacitor boost circuit for the switch on (100 μs from 0 to 15A), and TTL-controlled solid-state relays for the switch off (20 μs from 15A to zero current). An H-bridge switch electrically separates the two trapping coils, allowing a rapid switch of the direction of current in one of the coils (20 μs). The pair of coils dissipate an absolute maximum of 40 W total, and as a consequence no active cooling is required.

The experimental sequence is separated into three stages: loading of the atoms in the 3D MOT, evaporative cooling in the hybrid trap, and the interferometer sequence.

2.1. 3DMOT loading

At the end of a 10 s loading stage, 3×10^6 and 5×10^8 atoms of ^{85}Rb and ^{87}Rb respectively have been collected. Atom numbers are currently limited by our MOT beam size, and 2D-MOT

source flux. Following 25 ms of polarization gradient cooling (PGC) on both isotopes (smoothly decreasing magnetic field and repump intensity while increasing MOT detuning), the repump light is extinguished and 1ms later the trapping light is switched off, leaving a sample at a temperature of $\approx 15\ \mu$K. This sequence pumps both isotopes into their respective ground states. About 50% of the atoms accumulate in our target states of $|F = 1, m_F = -1\rangle$ for ^{87}Rb and $|F = 2, m_F = -2\rangle$ for ^{85}Rb.

2.2. Dual species, hybrid trap cooling

Immediately after PGC and optical pumping, the current in the trapping coils is switched on to capture the atoms in a quadrupole trap, and then ramped to full current over 100 ms, generating our maximum gradient of $\sim 300\,\mathrm{G\,cm^{-1}}$. Simultaneously with the magnetic field ramp up, the power from two separate laser beams, intersecting at 30°, is increased to produce a hybrid quadupole-magnetic and optical-dipole trap for the atoms. The axial confinement laser runs at $\lambda = 1090$ nm, with a 2 nm linewidth, 25 W power and beam waist 100 μm. The primary trapping laser (and waveguide) runs at $\lambda = 1064$ nm, with a 1 MHz linewidth, 20 W power and beam waist 60 μm. During 3.5 s, the magnetic and optical parameters of the hybrid trap are kept constant, while the clouds are cooled by radio frequency (rf) evaporation of ^{87}Rb atoms in the $|F = 1, m_F = -1\rangle$ ground state. The ^{85}Rb atoms in $|F = 2, m_F = -2\rangle$ are cooled sympathetically, due to their tighter confinement in the quadrupole magnetic field [24, 27]. The s-wave scattering lengths at this stage in the experiment are $a_{85} = -443a_0$, $a_{87} = 99a_0$ and $a_{85,87} = 213a_0$, where a_0 is the Bohr radius. The relatively large $a_{85,87}$ scattering length ensures good thermalization between the two species. The magnetic field is then ramped to zero over 3 s, loading the two isotopes into the pure crossed dipole trap, whilst forced rf evaporation continues until the magnetic field is off. At this stage we have a sample of 3.5×10^5 ^{85}Rb and 2.5×10^6 of ^{87}Rb atoms at temperatures close to 1 μK.

The H-bridge is then switched to the Helmholtz configuration, and the current is ramped up over 50 ms to provide a bias field of ~ 140 G, and then rapidly jumped through the 155 G Feshbach resonance to 165.64 G, zeroing the s-wave scattering length of ^{85}Rb and minimizing three-body loss [28, 29]. Over a further 3.5 s the dipole trap intensities are smoothly ramped down to their final value giving an optical trap with radial and axial trapping frequencies of 70 Hz and 9 Hz, respectively. In the last 0.5 s of this ramp the bias field is tuned to give a ^{85}Rb s-wave scattering length of 300 a_0. We set the scattering length to be large to increase the physical size of the cloud and to optimise miscibility/atom number. Pure BECs of 2×10^4 ^{85}Rb and 2×10^5 ^{87}Rb are formed at this stage. In the crossed dipole trap this results in condensates of radial and axial widths of 5.6(4.4) μm and 43(35) μm, respectively, for $^{87\,(85)}$Rb and a peak density of $10^{14\,(13)}$ $\mathrm{atoms\,cm^{-3}}$, calculated using the Thomas–Fermi (TF) approximation. 3D Numerical simulations, based on a system of radially symmetric Gross–Pitaevskii equations (without gravity), indicate a near complete phase separation at these parameters, with the ^{85}Rb atoms residing outside of the ^{87}Rb core, primarily along the radial direction. The peak ^{85}Rb atom density is reduced by a factor of 2, compared to the TF approximation. Depending on the details of the 3DMOT loading sequence, the condensate isotope ratio can be precisely controlled, from pure ^{87}Rb, through a mixture, to pure ^{85}Rb. Repeatability at about the level of 20% is achievable for both isotopes. Modification of the ^{85}Rb s-wave scattering length in the final optical cooling sequence allows condensates to be produced at a range of scattering lengths, including very near zero.

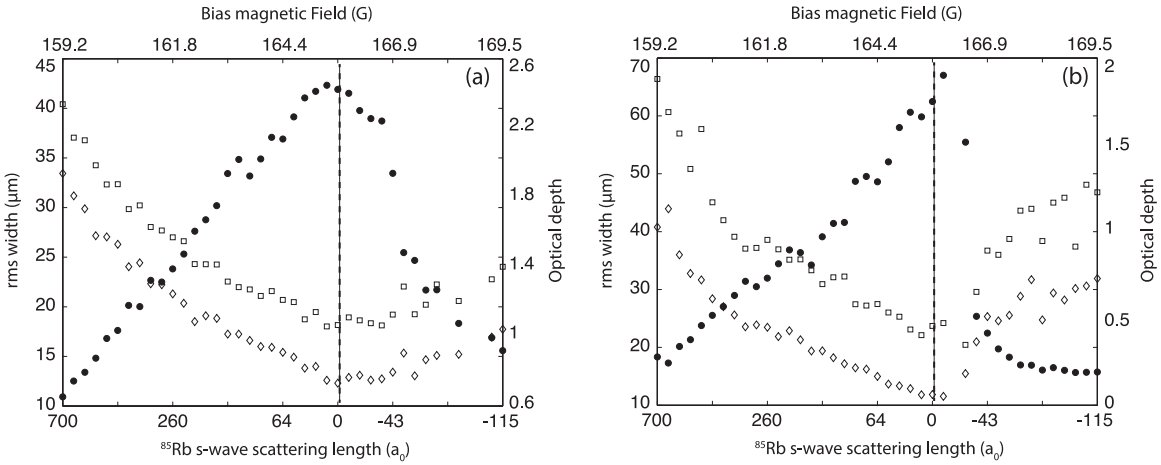

Figure 2. (a) Expansion of the ^{85}Rb condensate from the crossed dipole trap as a function of scattering length after the trap has turned off (the background magnetic field is also shown for reference). Filled circles—OD, squares—σ_x radial width, diamonds —σ_y axial width. Vertical dashed line indicates zero scattering length on the horizontal axis. (b) Expansion along the waveguide as a function of Feshbach magnetic field. Filled circles—OD, squares—σ_x radial width, diamonds—σ_y axial width. Both sets of data represent a single set of runs at different values of the magnetic field.

After creation of the dual species condensate, the ^{85}Rb s-wave scattering length can be tuned by varying the current in the Fechbach coils. Indeed, this tuneability is a key feature to reduce systematics in the latest space interferometer proposals [11, 12]. Figure 2(a) demonstrates the tuneable nature of the s-wave scattering length in ^{85}Rb. Here, the condensate is created at 300 a_0, and then the crossed dipole trap is turned off in ∼10 μs. Simultaneously, the Feshbach magnetic field is jumped to different values, rapidly changing the scattering length and hence the expansion rate of the condensate. Larger values of scattering length increase the 85 condensate mean-field energy, causing the cloud to expand rapidly and the optical depth to decrease, while smaller values cause the cloud to maintain or even decrease its size. At negative values of the scattering length, the condensate is known to rapidly collapse [30], with a signature heating (and requisite increase in size of the cloud). To observe this change in expansion rate, after 15 ms the Feshbach field is switched to zero and after a further 10ms expansion, the atoms are imaged with absorption imaging. The observed change in width is a feature of a tuneable scattering length condensate, and does not appear for a thermal cloud [31].

2.3. Transfer into the waveguide and the interferometer sequence

To perform the interferometer sequence, the atom clouds are transferred into a single beam dipole trap, effectively forming a waveguide for the atoms [32]. The loading sequence follows our previous technique [33], with the addition that, after forming the ^{85}Rb condensate, the scattering length is ramped to zero over 100 ms, followed by a ramp up in the power of the single beam dipole trap over 200 ms. The weaker cross beam is then switched off, releasing the clouds into the waveguide. It is observed that tuning the s-wave scattering length of the ^{85}Rb cloud to near zero mitigates heating in this transfer. Just prior to release, the radial and axial trapping frequencies are 70 Hz and ∼2 Hz, respectively. In the waveguide, just prior to switch off of the weak cross beam, the condensates have increased in axial length and decreased

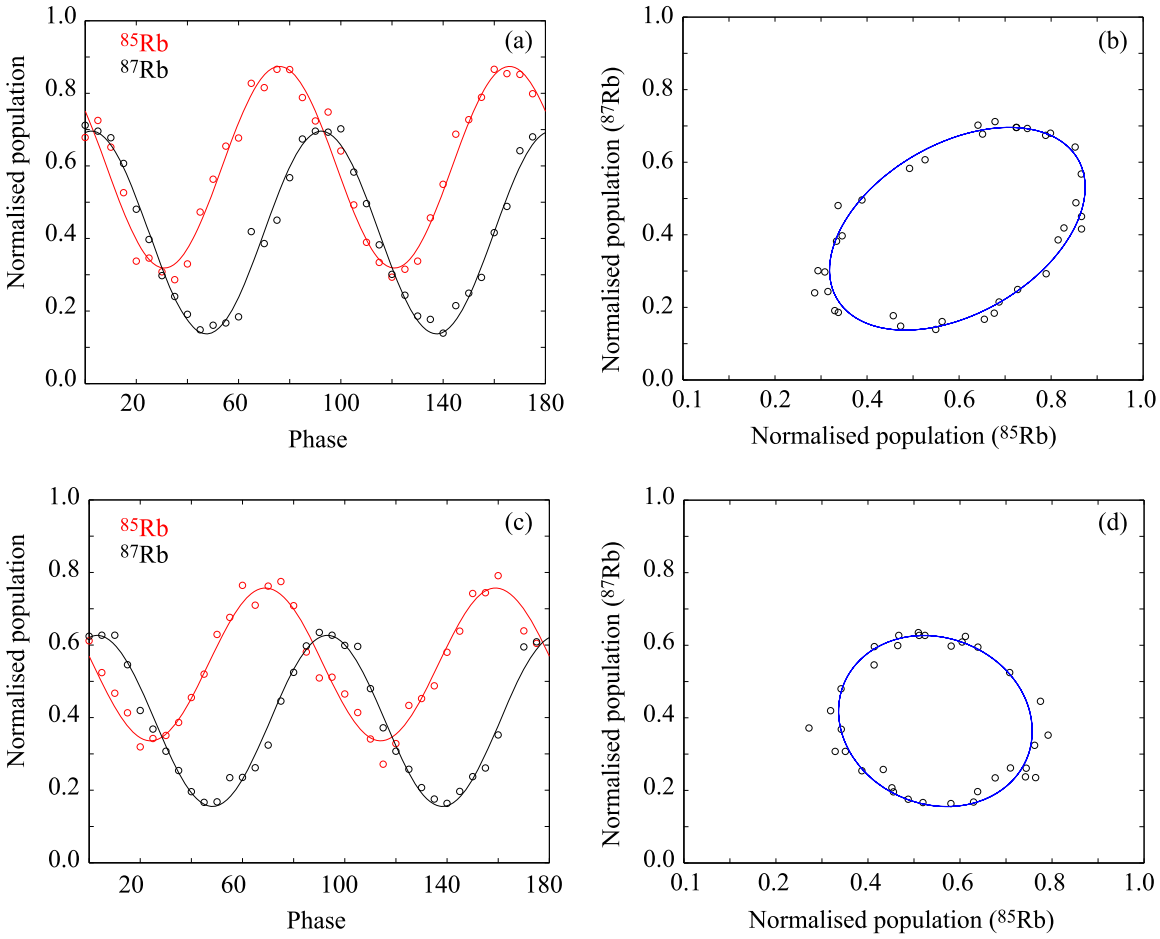

Figure 3. (a) and (c) show the simultaneous fringes acquired from a 0.4 ms and 0.5 ms interferometer, respectively. (b) and (d) show the ellipses generated from (a) and (c), respectively, by comparing normalized population in the two isotopes at varying phase.

slightly in radial extent, to have of radial and axial widths of 4.1(3.2) μm and 145(114) μm, respectively, for $^{87\,(85)}$Rb and a peak density of $10^{14\,(13)}$ atoms cm^{-3} , calculated using the TF approximation. 3D Numerical simulations, again based on a system of radially symmetric Gross–Pitaevskii equations (without gravity), indicate a near complete phase separation at these parameters, with the ^{85}Rb atoms residing outside of the ^{87}Rb core, primarily along the axial direction. The peak ^{85}Rb atom density is increased by a factor of 1.3, compared to the TF approximation. Using time-of-flight observations we have determined that the majority of the ^{87}Rb atoms initially occupy the transverse ground state of the waveguide [34]. Similarly to the release data from the crossed dipole trap, figure 2(b) shows expansion of the ^{85}Rb cloud in the waveguide. Recently such an expansion was described as the production of a 'bright soliton' in the region of small negative scattering length [35]. Additionally, RF sweeps similar to those used to calibrate the Feshbach magnetic field [24], can be used to transfer each isotope into any magnetic state [29, 36]. This will allow measurement of the interferometric phase shifts due to external magnetic fields, their gradients, and cross-and-self-scattering between the different m_F states of each isotope [37]. A systematic study is beyond the scope of this work, but is clearly an avenue for future experiments.

After release of the dual condensates into the waveguide, we engage a Bragg Mach–Zehnder interferometer. The Bragg optical setup consists of up to 50 mW in each of two counterpropagating beams, precisely aligned to the waveguide optical trap by means of dichroic mirrors [34]. The lattice beams are collimated with a full width of 1.85 mm and detuned ∼105 GHz to the blue from the D2 $|F=1\rangle \rightarrow |F'=2\rangle$ and $|F=2\rangle \rightarrow |F'=3\rangle$ transitions of ^{87}Rb and ^{85}Rb, respectively. Bragg beam polarization is optimized to achieve the largest Rabi frequency. Arbitrary, independent control of the frequency, phase, detuning, and amplitude of each beam is achieved using a two-channel direct digital synthesiser (DDS) driving two separate AOMs. The large detuning from both the ^{87}Rb and ^{85}Rb transitions sets the Bragg beamsplitter Rabi frequencies of the two isotopes equal to approximately 2%. For this work, beamsplitters and mirrors with up to $8\hbar k$ of momentum transfer, where $k = 2\pi/780.24$ nm is the single photon wavenumber, are used in a standard three pulse $\pi/2$, π, $\pi/2$ configuration, with each pair of pulses separated by a time, T. Atom numbers in the momentum state output ports of the interferometer are measured using simultaneous absorption imaging of each isotopes on (near) orthogonal horizontal axes.

This implementation of a Mach–Zehnder Bragg interferometer is primarily sensitive to external inertial forces [32, 33, 38], which lead to a phase shift on the interferometric fringes obtained. This phase shift is the 'signal' of the interferometer, which in our experiments is generated by (i) gravitational acceleration due to a small tilt in the horizontal waveguide, (ii) acceleration due to a small magnetic field curvature in the Helmholtz field and (iii) the mean field interaction between the two isotopes. Noise is generated by spurious accelerations of optical mirrors, vibration of the optical table and by possible fluctuating magnetic field gradients. This is particularly so in our system, since the waveguide laser strongly couples the atoms to these external noise sources at all times, as it is effectively tied to the laboratory. This is in contrast to free falling atoms, which form nearly ideal test masses. Figures 3(a), (c) shows typical interferometer fringes obtained by scanning the optical phase of the final Bragg beamsplitter. As observed in the laser-cooled simultaneous interferometer reported in [18], the fringes for each isotope indicate that they have acquired a different phase shift through the interferometer, but unlike that work, the fringes are of very similar contrast. We attribute the similarity in contrast of the fringes of each isotope to the use of Bragg transitions. The Bragg laser system has only a single frequency in each counter-propagating beam, and hence drives the atoms with near identical Rabi frequencies. The ellipses shown in figures 3(b), (d) are generated by parametrically plotting the normalized atom number of each isotope for every realization of the interferometer. The fact that some of the data lies off the fit to the ellipse indicates that there is non-common-mode noise between the two interferometers. Ideally, plotting the data parametrically should reject a significant amount of common noise [18] (such as vibration of the lab table). It is most likely that the outlying data originates primarily from classical noise that is observed in our absorption imaging, and this is clearly a candidate for improvement in the apparatus. Previously, we have experimentally observed shot noise limited interferometry with 10^4 ^{87}Rb [39] atoms, and in a separate paper we have calculated that an observable interferometric signal-to-noise of 10 000:1 is possible with standard absorption imaging [40, 41].

There is also a notable phase shift between the two isotopes in the data of figure 3. In order to investigate this shift, a ^{85}Rb Bragg interferometer is operated at zero s-wave scattering length, and the interferometric phase shift is studied as a function of the interferometer time, with different numbers of ^{87}Rb present. With negligible ^{87}Rb present, there is no obvious systematic

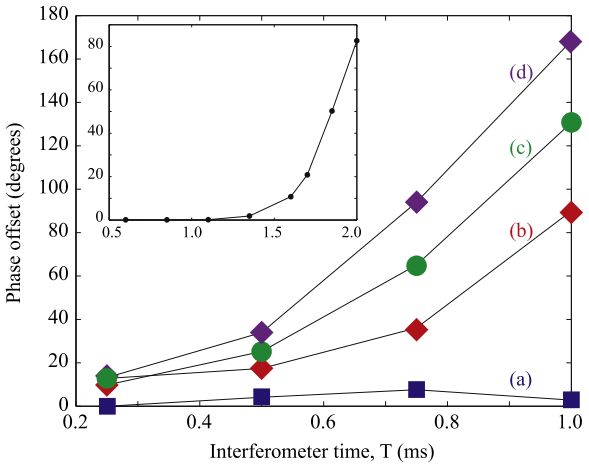

Figure 4. Phase shift on ^{85}Rb ($a_s \sim 0$) fringes as a function of interferometer time, T, in the waveguide, for varying atom number in the ^{87}Rb co-incident interferometer. (a) ~0 atoms in ^{87}Rb, (b) 3×10^4 atoms in ^{87}Rb, (c) 6×10^4 atoms in ^{87}Rb, (d) 10^5 atoms in ^{87}Rb. Inset: results of a numerical simulation based on a system of 1D Gross–Pitaevskii equations, showing qualitatively similar behaviour to the experiment for $N_{85} = 2 \times 10^4$ and $N_{87} = 1 \times 10^5$, $a_{85} = 0$, $a_{87} = 100a_0$ and $a_{85/87} = 213a_0$. A miscible initial condition in a 9 Hz trap is used for this simulation.

phase shift on the ^{85}Rb interferometer, as shown in figure 4, curve (a). However, as the number of ^{87}Rb atoms is increased there is a nonlinear increase in the phase shift of the ^{85}Rb interferometer. Reversing the wave-vectors of the Bragg beams, simply reverses the sign of this phase evolution, without changing its form.

A one-dimensional numerical simulation based on a system of coupled Gross–Pitaevskii equations [17] for the two isotopes can be used to make a qualitative investigation of the observed effect, since the system can be considered as a weakly interacting two component condensate with potentially complex initial conditions and dynamics [42, 43]. This simulation contains the $a_{85} = 0$ and $a_{87} = 99a_0$ intra- and $a_{85/87} = 213a_0$ inter-isotope s-wave scattering lengths. These simple numerical simulations indicate that there are complex spatial dynamics at play between the two isotopes. These spatial dynamics cause a nonlinear phase shift in ^{85}Rb due simply to the presence of ^{87}Rb, as shown in the inset to figure 4. There is no phase shift observed without ^{87}Rb present. Quantitive agreement between experiment and theory will require a full 3D simulation taking into account gravitational sag, which is beyond the scope of this paper but is needed to understand how this trapped system evolves over time, and more importantly, how expanded systems will evolve over the long interferometer times needed for WEP tests.

3. Discussion

In this work, we have presented a relatively simple arrangement to produce simultaneous ^{85}Rb and ^{87}Rb Bose–Einstein condensates. Following this, we have loaded the condensates into an optical waveguide and demonstrated the first simultaneous dual-species Bose-condensed atom interferometer. It is important to consider how our design and observations might contribute to

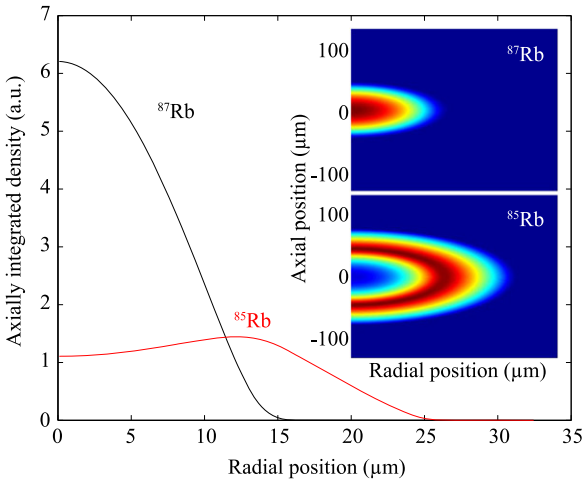

Figure 5. Miscibility does not imply complete interpenetration. Initial conditions that are predicted to be miscible by the simple equation $\mu = a_{85}a_{87}/a_{85,87}^2$ [25, 27]. Numerical solution of the radially symmetric GP equation for the ground states of a dual condensate system, in the absence of gravity. Parameters here are radial and axial trapping frequencies of 20 Hz and 7 Hz, respectively. Each condensate contains 10^6 atoms. S-wave scattering lengths used are $a_{85} = 1000a_0$, $a_{87} = 100a_0$ and $a_{85/87} = 213a_0$. The main plot shows the integrated profile of the two atom clouds, while the insets show the axial and radial density distribution.

discussions and planning on space-based and terrestrial precision measurement systems, such as the acceleration due to gravity or a violation of the WEP.

3.1. Initial conditions in the dual condensate system

The performance of a dual-species interferometer is highly dependent on having a clean initial spatial profile which evolves in a known way. Spatial dynamics driven by differences in scattering lengths can be complex and detrimental, and degrade interferometric performance, especially when the two species do not interpenetrate. We have previously mentioned that from the outcome of radially symmetric 3D numerical simulations, we expect the *initial condition* for our dual species atom interferometer to be immiscible. This situation is often characterized by the miscibility parameter, $\mu = a_{85}a_{87}/a_{85,87}^2$ [25, 27]. If $\mu < 1$, the interspecies repulsion overpowers the intra-species interaction, and the components will spatially separate. On the other hand, if $\mu > 1$ the two species will be miscible and the condensates will interpenetrate. Gravitational sag in the optical trap further complicates the initial conditions, as does the different magnetic moment of the initial states. There are strong caveats to this characterization, which have important implications for both space and terrestrial efforts to produce BEC based precision measurement systems. While the miscibility equation predicts interpenetrating condensates above a ^{85}Rb s-wave scattering length of $460a_0$, our numerical simulations indicate that there is still significant repulsion between the isotopes, even for dual condensate systems with $a_{85} = 1000a_0$. The numerical solution of the radially symmetric GP equation for the ground states of a *miscible* dual condensate system, in the absence of gravity, are shown in figure 5. For terrestrial precision measurement systems based on dual condensates the situation

is more complicated due to a relative gravitational sag in the optical trap. Clearly, significant further effort needs to be applied to understand and control spatial effects on the source clouds.

3.2. Systems for the production of condensates

Current proposals use a magnetic chip trap to generate the fields for the MOT, and for creating an Ioffe–Pritchard (IP) configuration harmonic trap for evaporative cooling [11, 12]. Here we have shown that a more complicated macroscopic IP trap can be dispensed with altogether, in favour of a single pair of coils that provide the field for the MOT, magnetic trap and Feshbach magnetic field. The configuration presented here may thus provide an alternative to a chip-based system, potentially providing greater optical access and simplicity than current designs. It should be noted however, that the hybrid optical/magnetic potential used for pre-cooling would need to be carefully considered for operation in zero gravity.

The number of condensed ^{85}Rb atoms proposed for both terrestrial-and space-based atom interferometer experiments exceed current state of the art by nearly two orders of magnitude. It is important to consider that to achieve fast and efficient sympathetic cooling of ^{85}Rb by ^{87}Rb in the pre-cooling stage requires a careful balance in atom number [25–27]. ^{85}Rb will not efficiently evaporatively cool by itself due to an extremely low collision cross-section around 100 μK [44], although it is feasible to produce condensates slowly [31, 45]. For the very large condensates being proposed, it is conceivable that lattice cooling [46, 47] will be required to overcome the stringent requirements placed on initial atom numbers by sympathetic cooling.

3.3. Comparing Raman and Bragg optical beam-splitters

Raman transitions are the mainstay of most atom interferometer precision measurement systems. It was recently shown that the Bragg transitions used in this work are compatible with an ultra-high precision measurement of gravity at the 3 ppb level [38]. There are a number of interesting differences between Bragg transitions and the proposed Raman laser systems for space missions. For Bragg transitions, (i) only two counter-propagating laser beams, each with a single frequency, are required to drive the dual isotope interferometer, giving good common mode noise rejection between the two isotope; (ii) only a single internal atomic state is used, reducing or eliminating many of the systematic effects common to all Raman based systems; (iii) detection via absorption imaging is simultaneous on all momentum states, reducing systematic effects on detection; and finally, (iv) large momentum transfer beam splitting offers the opportunity to increase the measurement sensitivity [48]. Enormous investments have been made in understanding systematic effects in Raman transitions. To provide an informed comparison, a similar study of systematic effects in high precision atom interferometry with Bragg transitions is required.

To illustrate this comparison, Raman transitions allow one to match the Rabi frequencies to 1 part in 10^4 using multiple laser frequencies [9–12]. There are two ways to approach this level of accuracy with Bragg. The first is to situate the Bragg frequency halfway between the ^{87}Rb $F = 1$ and ^{85}Rb $F = 2$ ground states, which are separated by about ~2 GHz. If the laser frequency was stabilised to ±100 kHz this would achieve the desired goal. The second method would be to detune the Bragg laser from both transitions by greater than 20THz. With our present setup we can drive Rabi frequencies of 1 MHz for a $2\hbar k$ transition. Thus we could achieve 5 kHz Rabi frequencies at 20 THz. With the 4 cm beams specified in the proposed space missions, we would require a factor of 400 higher power to achieve the same Rabi frequency,

giving a laser power requirement around 40 W. Note however, that we routinely achieve 12 W of power at 780 nm using single pass doubling of a 30 W 1560 nm fibre laser [49]. This laser could then be used for optical trapping at 1560 nm and then re-purposed for the Bragg lasers.

3.4. Which states to use in a precision measurement?

The internal states required for dual-species condensation of ^{85}Rb and ^{87}Rb are constrained by the scattering properties of ^{85}Rb and the requirements of sympathetic evaporative cooling [25]. However, once the condensates have been created in the pure optical dipole trap, the internal states used in the interferometer can be chosen freely. Indeed we have performed Ramsey interferometry on the $m_F = 0$ ground states of ^{87}Rb in this system [40, 41]. At high densities the choice for ^{85}Rb is restricted to the $|F = 2, m_F = -2\rangle$ state by the availability of the wide Feshbach resonance in this state, as the background scattering length of $a \approx -400a_0$ will cause such high density clouds to collapse [30]. In an expanded cloud in which the atoms do not collide with one another during the time of the interferometer, we are also free to choose any internal state for ^{85}Rb. If an experiment is planned using Raman transitions, then it would be clearly advantageous to use the $m_F = 0$ sub-levels of both ground states of ^{85}Rb and ^{87}Rb. As the internal magnetic state does not change in a Bragg interferometer, choosing the $m_F = 0$ sub-level of either of the ground states reduces the differential magnetic phase shift by a factor of 1/2 as compared with Raman.

4. Conclusion

In summary, an apparatus to produce a dual-species BEC atom interferometer with a 20 s repetition rate has been demonstrated. The condensates were loaded into a horizontal optical wave guide, where a Bragg Mach–Zehnder interferometer was applied. A relative phase shift driven by inter-isotope s-wave scattering was observed and numerically confirmed, although future 3D numerical studies will be required to gain a quantitative understanding of the system. Our technique for condensate production is readily applicable, and perhaps critical, to ongoing efforts to produce experimental data in the realm of predicted violations of the universality of free fall.

Avenues for further study include the production of a non-dispersive soliton atom interferometer [50], detailed 3D numerical studies of ^{85}Rb–^{87}Rb inter-isotope scattering and dynamics, and an investigation of systematic effects in a high-precision Bragg atom interferometer.

Acknowledgments

The authors gratefully acknowledge the support of the Australian Research Council Discovery program. CCNK would like to acknowledge financial support from CNPq (Conselho Nacional de Desenvolvimento Cientifico e Tecnologico). JED would like to acknowledge financial support from the IC postdoctoral fellowship program.

References

[1] Hall M J W, Reginatto M and Savage C M 2012 Nonlocal signaling in the configuration space model of quantum-classical interaction *Phys. Rev.* A **86** 054101

[2] Kiefer C 2012 *Quantum Gravity* 3rd edn (Oxford: Oxford University Press)

[3] Liberati S 2013 Tests of Lorentz invariance: a 2013 update *Class. Quantum Grav.* **30** 133001

[4] Dimopoulos S, Graham P W, Hogan J M and Kasevich M A 2007 Testing general relativity with atom interferometry *Phys. Rev. Lett.* **98** 111102

[5] Müller H, Chiow S-w, Herrmann S, Chu S and Chung K-Y 2008 Atom-interferometry tests of the isotropy of post-newtonian gravity *Phys. Rev. Lett.* **100** 031101

[6] Dimopoulos S and Geraci A A 2003 Probing submicron forces by interferometry of Bose–Einstein condensed atoms *Phys. Rev.* D **68** 124021

[7] Tarallo M G, Alberti A, Poli N, Chiofalo M L, Wang F-Y and Tino G M 2012 Delocalization-enhanced Bloch oscillations and driven resonant tunneling in optical lattices for precision force measurements *Phys. Rev.* A **86** 033615

[8] Schmidt M, Senger A, Hauth M, Freier C, Schkolnik V and Peters A 2011 A mobile high-precision absolute gravimeter based on atom interferometry *Gyroscopy and Navigation* **2** 170–7

[9] Tino G M *et al* 2013 Precision gravity tests with atom interferometry in space (Proceedings of the IV International Conference on Particle and Fundamental Physics in Space) *Nucl. Phys.* B **243–244** 203–17

[10] Sorrentino F *et al* 2011 The space atom interferometer project: status and prospects *J. Phys.: Conf. Ser.* **327** 12050

[11] Schubert C *et al* 2013 Differential atom interferometry with 87rb and 85rb for testing the UFF in STE-QUEST arXiv:1312.5963

[12] Aguilera D *et al* 2014 *Class. Quantum Grav.* **31** 115010

[13] Müntinga H *et al* 2013 Interferometry with Bose–Einstein condensates in microgravity *Phys. Rev. Lett.* **110** 093602

[14] Geiger R *et al* 2011 Detecting inertial effects with airborne matter-wave interferometry *Nat. Commun.* **2** 474

[15] Robins N P, Altin P A, Debs J E and Close J D 2013 Atom lasers: production, properties and prospects for precision inertial measurement *Phys. Rep.* **529** 265–96

[16] Lan S-Y, Kuan P-C, Estey B, Haslinger P and Müller H 2012 Influence of the Coriolis force in atom interferometry *Phys. Rev. Lett.* **108** 090402

[17] Hardman K S, Kuhn C C N, McDonald G D, Debs J E, Bennetts S, Close J D and Robins N P 2014 Role of source coherence in atom interferometery *Phys. Rev.* A **89** 023626

[18] Bonnin A, Zahzam N, Bidel Y and Bresson A 2013 Simultaneous dual-species matter-wave accelerometer *Phys. Rev.* A **88** 043615

[19] Berrada T, van Frank S, Bücker R, Schumm T, Schaff J-F and Schmiedmayer J 2013 Integrated Mach Zehnder interferometer for Bose–Einstein condensates *Nat. Commun.* **4** 2077

[20] Gustavsson M, Haller E, Mark M J, Danzl J G, Rojas-Kopeinig G and Nägerl H-C 2008 Control of interaction-induced dephasing of Bloch oscillations *Phys. Rev. Lett.* **100** 080404

[21] Fattori M, D'Errico C, Roati G, Zaccanti M, Jona-Lasinio M, Modugno M, Inguscio M and Modugno G 2008 Atom interferometry with a weakly interacting Bose–Einstein condensate *Phys. Rev. Lett.* **100** 080405

[22] Compton R L, Lin Y-J, Jimenez-Garcia K, Porto J V and Spielman I B 2012 Dynamically slowed collapse of a Bose–Einstein condensate with attractive interactions *Phys. Rev.* A **86** 063601

[23] Lin Y-J, Perry A R, Compton R L, Spielman I B and Porto J V 2009 Rapid production of ^{87}Rb Bose–Einstein condensates in a combined magnetic and optical potential *Phys. Rev.* A **79** 063631

[24] Altin P A, Robins N P, Doring D, Debs J E, Poldy R, Figl C and Close J D 2010 ^{85}Rb tunable-interaction Bose–Einstein condensate machine *Rev. Sci. Instrum.* **81** 063103

[25] Altin P A 2012 *PhD Thesis* Australian National University

[26] Papp S 2007 *PhD Thesis* University of Colorado

[27] Papp S B, Pino J M and Wieman C E 2008 Tunable miscibility in a dual-species Bose–Einstein condensate *Phys. Rev. Lett.* **101** 040402
[28] Roberts J L, Claussen N R, Cornish S L and Wieman C E 2000 Magnetic field dependence of ultracold inelastic collisions near a Feshbach resonance *Phys. Rev. Lett.* **85** 728–31
[29] Altin P A, Robins N P, Poldy R, Debs J E, Döring D, Figl C and Close J D 2010 Measurement of inelastic losses in a sample of ultracold Rb^{85} *Phys. Rev.* A **81** 012713
[30] Altin P A, Dennis G R, McDonald G D, Döring D, Debs J E, Close J D, Savage C M and Robins N P 2011 Collapse and three-body loss in a ^{85}Rb Bose–Einstein condensate *Phys. Rev.* A **84** 033632
[31] Marchant A L, Händel S, Hopkins S A, Wiles T P and Cornish S L 2012 Bose–Einstein condensation of ^{85}Rb by direct evaporation in an optical dipole trap *Phys. Rev.* A **85** 053647
[32] Vermersch F, Fabre C M, Cheiney P, Gattobigio G L, Mathevet R and Guéry-Odelin D 2011 Guided-atom laser: transverse mode quality and longitudinal momentum distribution *Phys. Rev.* A **84** 043618
[33] McDonald G D, Kuhn C C N, Bennetts S, Debs J E, Hardman K S, Johnsson M, Close J D and Robins N P 2013 80$\hbar k$ momentum separation with Bloch oscillations in an optically guided atom interferometer *Phys. Rev.* A **88** 053620
[34] McDonald G D, Keal H, Altin P A, Debs J E, Bennetts S, Kuhn C C N, Hardman K S, Johnsson M T, Close J D and Robins N P 2013 Optically guided linear Mach–Zehnder atom interferometer *Phys. Rev.* A **87** 013632
[35] Marchant A L, Billam T P, Wiles T P, Yu M M H, Gardiner S A and Cornish S L 2013 Controlled formation and reflection of a bright solitary matter-wave *Nat. Commun.* **4** 1865
[36] Blackley C L, le Sueur C R, Hutson J M, McCarron D J, Köppinger M P, Cho H-W, Jenkin D L and Cornish S L 2013 Feshbach resonances in ultracold ^{85}Rb *Phys. Rev.* A **87** 033611
[37] Rakonjac A, Deb A B, Hoinka S, Hudson D, Sawyer B J and Kjærgaard N 2012 Laser based accelerator for ultracold atoms *Opt. Lett.* **37** 1085–7
[38] Altin P A *et al* 2013 Precision atomic gravimeter based on Bragg diffraction *New J. Phys.* **15** 023009
[39] Döring D, McDonald G, Debs J E, Figl C, Altin P A, Bachor H-A, Robins N P and Close J D 2010 Quantum-projection-noise-limited interferometry with coherent atoms in a Ramsey-type setup *Phys. Rev.* A **81** 043633
[40] Altin P A, McDonald G, Döring D, Debs J E, Barter T H, Close J D, Robins N P, Haine S A, Hanna T M and Anderson R P 2011 Optically trapped atom interferometry using the clock transition of large ^{87}Rb Bose–Einstein condensates *New J. Phys.* **13** 065020
[41] Altin P A, McDonald G, Döring D, Debs J E, Barter T H, Robins N P, Close J D, Haine S A, Hanna T M and Anderson R P 2011 Optically trapped atom interferometry using the clock transition of large ^{87}Rb Bose–Einstein condensates *New J. Phys.* **13** 119401
[42] Stamper-Kurn D M and Ueda M 2013 Spinor Bose gases: symmetries, magnetism, and quantum dynamics *Rev. Mod. Phys.* **85** 1191–244
[43] Pattinson R W, Billam T P, Gardiner S A, McCarron D J, Cho H W, Cornish S L, Parker N G and Proukakis N P 2013 Equilibrium solutions for immiscible two-species Bose–Einstein condensates in perturbed harmonic traps *Phys. Rev.* A **87** 013625
[44] Burke J P, Bohn J L, Esry B D and Greene C H 1998 Prospects for mixed-isotope Bose–Einstein condensates in rubidium *Phys. Rev. Lett.* **80** 2097–100
[45] Cornish S L, Claussen N R, Roberts J L, Cornell E A and Wieman C E 2000 Stable ^{85}Rb Bose–Einstein condensates with widely tunable interactions *Phys. Rev. Lett.* **85** 1795–8
[46] Olshanii M and Weiss D 2002 Producing Bose–Einstein condensates using optical lattices *Phys. Rev. Lett.* **89** 090404
[47] Li X, Corcovilos T A, Wang Y and Weiss D S 2012 3D projection sideband cooling *Phys. Rev. Lett.* **108** 103001
[48] McDonald G D, Kuhn C C N, Bennetts S, Debs J E, Hardman K S, Close J D and Robins N P 2014 A faster scaling in acceleration-sensitive atom interferometers *Europhys. Lett.* **105** 63001

[49] Sané S S, Bennetts S, Debs J E, Kuhn C C N, McDonald G D, Altin P A, Close J D and Robins N P 2012 11 w narrow linewidth laser source at 780 nm for laser cooling and manipulation of rubidium *Opt. Express* **20** 8915–9

[50] McDonald G D *et al* 2014 A bright solitonic matter-wave interferometer *Phys. Rev. Lett.* **113** 013002